JCTC Journal of Chemical Theory and Computation

Article

Cite This: J. Chem. Theory Comput. XXXX, XXX, XXX−XXX

pubs.acs.org/JCTC

The Importance of Cell Shape Sampling To Accurately Predict Flexibility in Metal−Organic Frameworks

Sven M. J. Rogge,[†] Senne Caroes,[†] Ruben Demuynck, Michel Waroquier, Veronique Van Speybroeck, and An Ghysels*

Center for Molecular Modeling (CMM), Ghent University, Technologiepark 903, 9052 Zwijnaarde, Belgium

Supporting Information

ABSTRACT: In this work, the influence of cell shape sampling on the predicted stability of the different metastable phases in flexible metal−organic frameworks at finite temperatures is investigated. The influence on the free energy by neglecting cell shape sampling is quantified for the prototypical MIL-53(Al) and the topical DUT-49(Cu). This goal is achieved by constructing free energy profiles in ensembles either in which the phase space associated with the cell shape is sampled explicitly or in which the cell shape is kept fixed. When neglecting cell shape sampling, thermodynamic integration of the hydrostatic pressure yields unreliable free energy profiles that depend on the choice of the fixed cell shape. In this work, we extend the thermodynamic integration procedure via the introduction of a generalized pressure, derived from the Lagrangian strain tensor and the second Piola−Kirchhoff tensor. Using this generalized procedure, the dependence on the unit cell shape can be eliminated, and the inaccuracy in free energy stemming from the lack of cell shape sampling can be uniquely quantified. Finally, it is shown that the inaccuracy in free energy when fixing the cell shape at room temperature stems mainly from entropic contributions for both MIL-53(Al) and DUT-49(Cu).

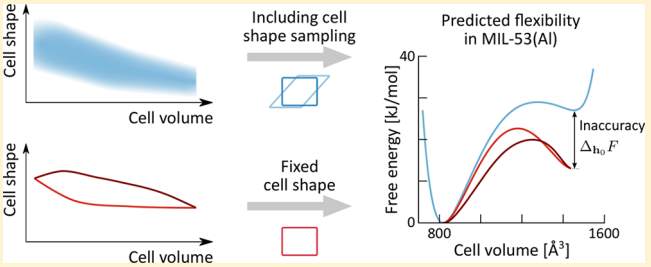

1. INTRODUCTION

Metal−organic frameworks (MOFs) or porous coordination polymers form a class of nanoporous yet crystalline materials formed by metal oxide clusters at the nodal points, which are interconnected by organic ligands.[1−3] Because of their scaffold-like structure and large inner surface area, MOFs have drawn widespread attention for applications in, e.g., heterogeneous catalysis,[4] controlled drug release,[5] and gas storage and separation.[6,7] More recently, the advent of flexible MOFs, which may undergo structural transitions under the influence of external stimuli such as temperature, pressure, and guest adsorption, also opened the pathway for possible MOF applications as nanodampers or in chemical sensing.[8,9] Especially interesting for these applications are the so-called breathing MOFs, which undergo reversible, large-amplitude volume changes upon phase transitions under external stimuli.[10] This breathing behavior can, moreover, be tuned by anion or cation exchange, giving rise to a versatility of flexible MOFs.[11−13] This engineering of the flexibility paves the way to tune flexible MOFs for targeted applications, provided that a clear understanding of the microscopic factors triggering flexibility is present.

One of the earliest series of MOFs in which the breathing behavior was investigated extensively is the MIL-53 family.[14] In this family of materials, transitions between a large-pore (lp) phase and a closed-pore (cp) phase can be induced experimentally by temperature and pressure changes (see Figure 1a),[15−17] and a narrow-pore (np) phase with intermediate volumes can be reached by gas adsorption.[14] The typical winerack topology in MIL-53(Al), formed by parallel, infinite aluminum hydroxide $[Al(OH)]_\infty$ chains connected through 1,4-benzenedicarboxylate (BDC) ligands, endows this material with the topological freedom to exhibit transitions between the lp and cp phases without breaking or creating bonds. On a microscopic level, the breathing in MIL-53(Al) is associated with a kneecap motion around the carboxylate oxygens.[18,19] Since these initial studies, breathing has been encountered in multiple MOFs,[10] one of the most recent being DUT-49(Cu).[20] DUT-49(Cu) is composed of copper paddlewheel units connected through 9,9′-([1,1′-biphenyl]-4,4′-diyl)bis(9*H*-carbazole-3,6-dicarboxylate) (BBCDC) ligands and was shown to exhibit negative gas adsorption for methane, *n*-butane, and xenon.[21,22] This negative gas adsorption is associated with a phase transition from the open-pore (op) to the closed-pore (cp) phase (see Figure 1b).[23] Computational investigation of the phase transition in DUT-49(Cu) revealed that the transition can also be induced by pressure and is associated on the microscopic scale with a buckling of the BBCDC ligand.[23]

Given the versatility of flexible MOFs, computational modeling has proven vital to rationalize this flexibility and to obtain insight into the microscopic parameters favoring this behavior.[8,24] On a thermodynamic level, flexibility is identified

Received: November 10, 2017
Published: February 14, 2018

DOI: 10.1021/acs.jctc.7b01134
J. Chem. Theory Comput. XXXX, XXX, XXX−XXX

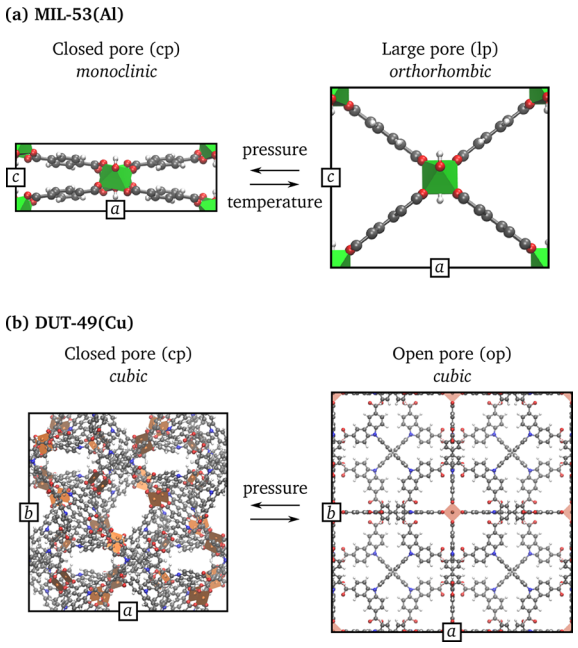

Figure 1. Breathing transformation between (a) the orthorhombic large-pore and the monoclinic closed-pore phase of MIL-53(Al) and (b) the cubic open-pore and the cubic closed-pore phase of DUT-49(Cu). Color code: copper unit (brown), aluminum unit (green), oxygen (red), carbon (gray), and hydrogen (white).

by the presence of multiple (meta)stable phases at a given temperature, pressure, and guest loading, which are found as (local) minima in the free energy profile as a function of a well-chosen collective variable.[25−30] Recently, free energy profiles as a function of the volume, $F(V)$, have been derived for multiple rigid and flexible MOFs.[19,23,29,31,32] These profiles make it possible to follow the relative stability of the different (meta)stable phases at varying thermodynamic conditions, revealing flexibility induced by various external stimuli, such as pressure, temperature, or guest adsorption,[30] and were validated to be in quantitative agreement with experiment. As outlined in ref 32, these free energy profiles can be determined using a variety of advanced molecular dynamics (MD) methods, including thermodynamic integration (TI),[19,33] umbrella sampling (US),[34] and metadynamics (MTD).[35]

Essential in the sampling procedure are the degrees of freedom (DOFs) that are allowed to fluctuate during the MD simulation and hence specify the available phase space to be explored during the simulation. In general, this phase space is not only formed by the atomic positions $\{\boldsymbol{r}_i\}$ and momenta $\{\boldsymbol{p}_i\}$ but also by the cell matrix $\mathbf{h}$ containing the cell vectors. $\mathbf{h}$ defines the repeated unit cell in MD simulations, allowing for the application of periodic boundary conditions to mimic bulk materials without unphysical termination.[36,37] For isotropic systems, such as fluids, the only physically relevant DOF associated with the cell matrix is its volume $V = \det(\mathbf{h})$, as no shape-altering shear stresses can be present. In contrast, for anisotropic systems such as MOFs, the cell shape $\mathbf{h}_0 = \mathbf{h}/\sqrt[3]{V}$ can vary substantially. For instance, the lp-to-cp transition in MIL-53(Al), depicted in Figure 1a, corresponds with a transformation from the orthorhombic lp phase to the monoclinic cp phase. Sampling of these shape-altering motions, which will henceforth be referred to as "cell shape sampling", thus seems to be a prerequisite to accurately describe flexible MOFs for which the metastable phases differ in symmetry. For DUT-49(Cu), however, the cubic symmetry of the unit cell is retained during the phase transition from the op to the cp phase, and free energy profiles were previously constructed without cell shape sampling.[23] As it is computationally more efficient to reduce the number of DOFs to be sampled and therefore to fix the cell shape, it is important to know to which extent correct cell shape sampling is necessary to derive accurate free energy profiles for flexible materials.

Herein, we tackle this question by studying the influence of explicit cell shape sampling on the free energy profiles derived for both MIL-53(Al) and DUT-49(Cu), as schematically depicted in Figure 2. Specifically, the inaccuracy $\Delta_{\mathbf{h}_0}F$ in the

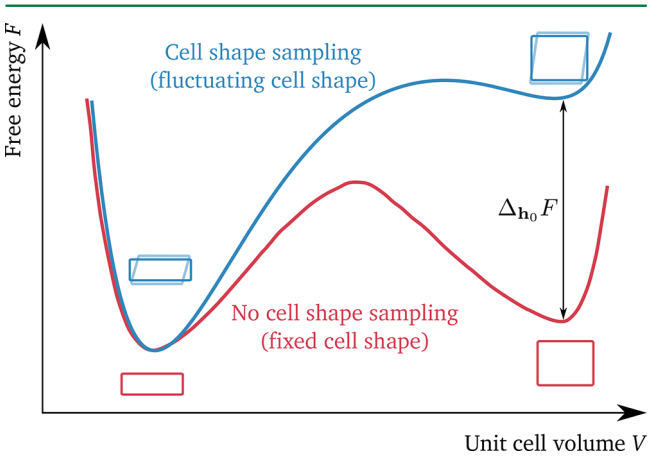

Figure 2. Schematic free energy profiles, F, as a function of the volume, V, for a flexible material, calculated in a thermodynamic ensemble for which the cell shape, $\mathbf{h}_0$, is either allowed to fluctuate (blue) or is kept fixed during the simulation (red). The two profiles are shifted to coincide at the lowest free energy minimum. The difference in the predicted relative stability of the metastable phase between the two methods, $\Delta_{\mathbf{h}_0}F$, determines the inaccuracy introduced by neglecting cell shape sampling.

free energy difference between the metastable phases introduced by neglecting proper cell shape sampling is quantified. We show that the inaccuracy can be associated with entropic rather than enthalpic contributions for both materials at room temperature. Furthermore, for those simulations during which the cell shape is fixed, it will be investigated how different choices of the fixed cell shape $\mathbf{h}_0$ may lead to widely differing results when directly applying thermodynamic integration of the pressure, P. However, by generalizing the derivation of thermodynamic integration for flexible MOFs discussed in ref 19, we demonstrate that a generalized pressure, P_a, can be derived from the second Piola−Kirchhoff tensor and the Lagrangian strain. This generalized pressure explicitly accounts for the effect of anisotropic stresses during simulations with a fixed cell shape. The new procedure allows us to quantify the inaccuracy $\Delta_{\mathbf{h}_0}F$, revealing that it is of the same order of magnitude as the difference in stability of the metastable states of MIL-53(Al). As a result, one should fully take cell shape sampling into account when generating free energy equations of state and predicting flexibility.

2. METHODOLOGY

To investigate the effect of cell shape sampling on the free energy profiles of MIL-53(Al) and DUT-49(Cu) and the

DOI: 10.1021/acs.jctc.7b01134
J. Chem. Theory Comput. XXXX, XXX, XXX−XXX

predicted flexibility of these materials, free energy profiles are constructed in different thermodynamic ensembles. First, in section 2.1, we shortly revisit the classification of thermodynamic ensembles previously established in ref 19 and properly introduce the relevant thermodynamic variables. Here, we distinguish between ensembles in which the phase space associated with the cell shape is sampled in section 2.2, and those in which the cell shape is kept fixed in section 2.3. For the latter, we introduce a generalized thermodynamic integration procedure, based on a generalized pressure, to account for the presence of nonvanishing deviatoric stresses in the material. For the two MOFs studied here, force field models that correctly describe the transition between the different (meta)stable states are available, so that we can focus solely on the error introduced by neglecting cell shape sampling. In general, however, it is essential to validate that the theoretical model accurately reproduces the experimental transition to preclude additional sources of inaccuracies in the free energy profile.

2.1. Thermodynamic Ensembles. Due to their periodic, scaffold-like structure, MOFs are often very anisotropic. This is for instance exemplified by the lp-to-cp transition in MIL-53(Al), shown in Figure 1a, in which the symmetry of the material changes. As a result, the volume alone, which represents only one degree of freedom, is not sufficient to fully describe the changes in the unit cell during the phase transition. Hence, the full cell matrix $\mathbf{h}$, composed of the unit cell vectors $\boldsymbol{a}$, $\boldsymbol{b}$, and $\boldsymbol{c}$, should be introduced. This 3 × 3 matrix contains nine components, of which three components describe the orientation of the unit cell in space. Of the remaining six physical degrees of freedom, one is associated with the cell volume, $V = \det(\mathbf{h})$, and the other five are associated with the cell shape

$$\mathbf{h}_0 = \mathbf{h}/\sqrt[3]{V} \tag{2.1}$$

for which $\det(\mathbf{h}_0) = 1$. Often, the cell matrix $\mathbf{h}$ is assumed to be a symmetric or an upper triangular matrix, in which case the six relevant degrees of freedom are readily apparent. In this work, we opted to symmetrize $\mathbf{h}$.

Likewise, given the anisotropy of MOFs, it makes sense to study the behavior of these materials under a given (Cauchy) stress, $\boldsymbol{\sigma}$, rather than only under a hydrostatic pressure, $P = \mathrm{Tr}(\boldsymbol{\sigma})/3$. The 3 × 3 symmetric stress matrix, $\boldsymbol{\sigma}$, contains six independent degrees of freedom: one assigned to P and five assigned to the traceless deviatoric stress matrix $\boldsymbol{\sigma}_a$:

$$\boldsymbol{\sigma}_a = \boldsymbol{\sigma} - P\mathbf{1} \tag{2.2}$$

where $\mathbf{1}$ is the identity matrix of size 3. The deviatoric stress matrix contains the anisotropic contributions to the total stress matrix. Note that, in general, $\mathbf{h}$ and $\boldsymbol{\sigma}$ are not thermodynamically conjugate variables.

The above-defined thermodynamic variables are external variables that are imposed on the system such as the temperature, T, and the pressure, P. For each of these properties, one can also define the corresponding internal variables, which are instantaneous properties of the system, such as the instantaneous internal temperature, T_i, and the instantaneous internal pressure, P_i. In general, even if we fix the external variables, the corresponding internal variables are still allowed to fluctuate. However, in equilibrium, they need to average out to their imposed external values.[19,37,38] For instance, in a constant-temperature, constant-pressure ensemble, equilibrium requires that $\langle P_i \rangle = P$ and $\langle T_i \rangle = T$.

To study the effect of cell shape sampling on the prediction of free energy profiles, we distinguish between three thermodynamic ensembles, as indicated in Table 1. In these ensembles, the number of particles, N, is kept fixed, and the temperature, T, is controlled such that the atomic velocities follow a Maxwell−Boltzmann distribution. For both the (N, P, $\boldsymbol{\sigma}_a = \mathbf{0}$, T) and the (N, V, $\boldsymbol{\sigma}_a = \mathbf{0}$, T) ensembles (see section 2.2), the deviatoric stress $\boldsymbol{\sigma}_a$ is controlled to be on average zero, resulting in a fluctuating unit cell shape $\mathbf{h}_0$. In addition, the pressure P is controlled in the (N, P, $\boldsymbol{\sigma}_a = \mathbf{0}$, T) ensemble, such that the unit cell volume V can fluctuate. In contrast, the cell volume is kept fixed in the (N, V, $\boldsymbol{\sigma}_a = \mathbf{0}$, T) ensemble. Finally, for the (N, V, $\mathbf{h}_0$, T) ensemble (see section 2.3), often referred to as the NVT ensemble, not only the cell volume V but also the cell shape $\mathbf{h}_0$ is kept fixed, which in general induces a nonvanishing deviatoric stress $\boldsymbol{\sigma}_a$.

Table 1. Overview of the Thermodynamic Ensembles and the Various Methods To Construct Free Energy Profiles in This Work, with Indication of Whether the Unit Cell Volume, V, and Unit Cell Shape, $\mathbf{h}_0$, Are Sampled and How the Cell Shape Is Obtained

ensemble	method	V sampled?	$\mathbf{h}_0$ sampled?	choice of $\mathbf{h}_0$
(N, P, $\boldsymbol{\sigma}_a = \mathbf{0}$, T)	MTD	yes	yes	–
(N, V, $\boldsymbol{\sigma}_a = \mathbf{0}$, T)	$\mathrm{TI}_{\mathrm{full}}$	no[a]	yes	–
(N, V, $\mathbf{h}_0$, T)	$\mathrm{TI}_{\mathbf{h}_0}^{\mathrm{snap}}$	no[a]	no	snapshot from MTD simulation
(N, V, $\mathbf{h}_0$, T)	$\mathrm{TI}_{\mathbf{h}_0}^{\mathrm{mean}}$	no[a]	no	mean from $\mathrm{TI}_{\mathrm{full}}$ simulation at V
(N, V, $\mathbf{h}_0$, T)	$\mathrm{TI}_{\mathbf{h}_0}^{\mathrm{ipol}}$	no[a]	no	interpolation between (meta)stable states

[a]While the volume is not sampled in each separate TI simulation, explicit volume sampling is performed by the a posteriori thermodynamic integration of the pressure.

2.2. Ensembles with Cell Shape Sampling: the (N, P, $\boldsymbol{\sigma}_a = \mathbf{0}$, T) and (N, V, $\boldsymbol{\sigma}_a = \mathbf{0}$, T) Ensembles. *2.2.1. Metadynamics in the (N, P, $\boldsymbol{\sigma}_a = \mathbf{0}$, T) Ensemble.* In the (N, P, $\boldsymbol{\sigma}_a = \mathbf{0}$, T) ensemble, the temperature and stress are controlled, mimicking the experimental conditions. In this ensemble, both the cell volume V and the cell shape $\mathbf{h}_0$ are sampled explicitly. However, given the free energy barrier between the two (meta)stable states, one has to rely on a biased molecular dynamics scheme to efficiently and reliably sample the activated phase transformation. Here, we opted to use metadynamics (MTD),[35] which was employed previously to study the hydrothermal breakdown of MIL-53(Ga)[39] and the lp-to-cp transition in MIL-53(Al).[32] During an MTD simulation, a history-dependent bias potential is gradually added to the system to promote the full exploration of the relevant phase space. This bias is a function of the collective variables that describe the transition of interest. Given the large change in unit cell volume between the two (meta)stable phases in both MIL-53(Al) and DUT-49(Cu), we chose V as the only collective variable. Upon convergence of the accumulated bias potential, its negative renders the free energy profile as a function of the volume and can be used to investigate the flexibility in these materials.

2.2.2. Thermodynamic Integration in the (N, V, $\boldsymbol{\sigma}_a = \mathbf{0}$, T) Ensemble. A second technique to study phase transformations

DOI: 10.1021/acs.jctc.7b01134
J. Chem. Theory Comput. XXXX, XXX, XXX−XXX

was introduced in ref 19. Herein, a series of parallel $(N, V, \boldsymbol{\sigma}_a = \mathbf{0}, T)$ simulations are performed at the volume range of interest. In each of these simulations, the cell volume is kept fixed, but the cell shape is allowed to fluctuate with the constraint that the deviatoric stress vanishes: $\boldsymbol{\sigma}_a = \mathbf{0}$. Since the cell volume is kept fixed, the average internal pressure, $\langle P_i \rangle$, the material exerts on its environment is, in general, nonzero. Assuming mechanical equilibrium, this pressure coincides with the external pressure P that needs to be exerted on the material to yield a volume V. From this set of $(N, V, \boldsymbol{\sigma}_a = \mathbf{0}, T)$ simulations, a macroscopic pressure-versus-volume $P(V)$ equation of state can be generated. This technique was, among others, adopted to study phase transformations in the MIL-53(Al) and MIL-47(V) families and amorphization in the UiO-66 series.[19,29,31]

Based on the obtained $P(V)$ equation of state, the free energy equation of state, $F(V)$, can be obtained by thermodynamic integration:[33]

$$F(V) - F(V_{\text{ref}}) = \int_{V_{\text{ref}}}^{V} \frac{\partial F(V')}{\partial V'} \, \mathrm{d}V' = -\int_{V_{\text{ref}}}^{V} P(V') \, \mathrm{d}V' \tag{2.3}$$

To draw attention to the fact that cell shape fluctuations are fully taken into account with this methodology, the free energy profiles resulting from the $(N, V, \boldsymbol{\sigma}_a = \mathbf{0}, T)$ ensemble are denoted with TI_{full}.

2.3. Generalized Pressure To Account for Anisotropic Stresses $\boldsymbol{\sigma}_a \neq \mathbf{0}$. When performing simulations in the $(N, V, \mathbf{h}_0, T)$ ensemble, the cell shape $\mathbf{h}_0$ is fixed, which generally induces a deviatoric stress $\boldsymbol{\sigma}_a$. As a result, P and V are no longer conjugate variables determining the free energy associated with a volume change: $\mathrm{d}F \neq -P \, \mathrm{d}V$. The aim of this section is to extend the thermodynamic integration procedure of section 2.2.2 by deriving a generalized pressure P_a that takes into account the deviatoric stress $\boldsymbol{\sigma}_a$ such that $\mathrm{d}F = -P_a \, \mathrm{d}V$. This generalized pressure P_a can then be readily integrated to obtain the free energy profile $F(V)$. To distinguish between the free energy profiles obtained with the TI_{full} method of section 2.2, the free energy profiles determined via thermodynamic integration of either the pressure P or the generalized pressure P_a in the $(N, V, \mathbf{h}_0, T)$ ensemble is denoted $\text{TI}_{\mathbf{h}_0}$, highlighting the fact that the cell shape was kept fixed during these simulations.

2.3.1. Derivation of P_a. Consider a system in a reference configuration, with corresponding cell matrix $\mathbf{h}_{\text{ref}}$ and cell volume $V_{\text{ref}} = \det(\mathbf{h}_{\text{ref}})$. Any deformation of this reference cell matrix $\mathbf{h}_{\text{ref}}$ to a deformed cell matrix $\mathbf{h}$ can be described by the finite Lagrangian strain tensor[40]

$$\boldsymbol{\eta} = \frac{1}{2}(\mathbf{F}^{\mathrm{T}}\mathbf{F} - \mathbf{1}) \tag{2.4}$$

Here, the deformation gradient $\mathbf{F}$ is defined as

$$\mathbf{F} = \mathbf{h}\mathbf{h}_{\text{ref}}^{-1} \tag{2.5}$$

where $\mathbf{A}^{\mathrm{T}}$ and $\mathbf{A}^{-1}$ denote the matrix transpose and matrix inverse of $\mathbf{A}$, respectively.

As outlined in ref 41, the free energy difference between the deformed cell $\mathbf{h}$ and the reference cell $\mathbf{h}_{\text{ref}}$ can then be determined by the integral

$$F(\mathbf{h}) - F(\mathbf{h}_{\text{ref}}) = -V_{\text{ref}} \int_{\boldsymbol{\eta}(\mathbf{h}_{\text{ref}})}^{\boldsymbol{\eta}(\mathbf{h})} \mathbf{S} : \mathrm{d}\boldsymbol{\eta}' \tag{2.6}$$

Here, $\mathbf{S}$ is the second Piola−Kirchhoff tensor, which relates to the Cauchy stress $\boldsymbol{\sigma}$ via

$$\mathbf{S} = \det(\mathbf{F})\mathbf{F}^{-1}\boldsymbol{\sigma}\mathbf{F}^{-T} \tag{2.7}$$

where ":" denotes the Frobenius inner product of two matrices; i.e., $\mathbf{A} : \mathbf{B} = \sum_{ij} A_{ij}B_{ij}$, and $\mathbf{A}^{-\mathrm{T}} = [\mathbf{A}^{-1}]^{\mathrm{T}}$. Given the expression in eq 2.6, $\mathbf{S}$ and $V_{\text{ref}}\boldsymbol{\eta}$ are the conjugate variables determining the free energy associated with a deformation under a nonhydrostatic stress $\boldsymbol{\sigma}$. Both $\mathbf{S}$ and $\boldsymbol{\eta}$ are related to the cell matrix $\mathbf{h}$ through the deformation gradient via eqs 2.4 and 2.5.

In eq 2.3, a free energy difference was defined with the volume as the only variable, while all other degrees of freedom, including the cell shape $\mathbf{h}_0$, were sampled. An analogous expression can be obtained from eq 2.6 if we assume a mapping from the cell volume to the cell shape: $\mathbf{h}_0 : V \rightarrow \mathbf{h}_0(V)$. In general, a material can exhibit multiple cell shapes at a given cell volume. As a result, multiple mappings exist; different choices for this mapping are further outlined in section 2.3.2 for MIL-53(Al) and DUT-49(Cu). When assuming such a mapping procedure, we can identify eq 2.6, obtained for a general stress, with the simplified eq 2.3, valid only for hydrostatic pressures. This yields the free energy difference with fixed cell shape as

$$F(V) - F(V_{\text{ref}}) = -\int_{V_{\text{ref}}}^{V} P_a(V') \, \mathrm{d}V' \tag{2.8}$$

in which

$$P_a = V_{\text{ref}}\mathbf{S} : \frac{\mathrm{d}\boldsymbol{\eta}}{\mathrm{d}V} = \frac{V_{\text{ref}}}{2}\mathbf{S} : \left(\frac{\mathrm{d}\mathbf{F}^{\mathrm{T}}}{\mathrm{d}V}\mathbf{F} + \mathbf{F}^{\mathrm{T}}\frac{\mathrm{d}\mathbf{F}}{\mathrm{d}V}\right) \tag{2.9}$$

has the dimension of pressure and can be regarded as a pressure-like quantity that is corrected for anisotropic stress.

In this derivation, it is assumed that the full Lagrangian strain, $\boldsymbol{\eta}$, and hence, through eqs 2.4 and 2.5, the full cell matrix, can be determined as a function of the volume V. In other words, this method requires that the cell shape $\mathbf{h}_0$ is chosen as a function of the cell volume V. In practice, this can be ensured by employing an interpolation scheme between the two (meta)stable states, as outlined below. The derivation shows that when $\mathbf{h}_0$ is written as a function of the volume through a continuous path $V \rightarrow \mathbf{h}_0(V)$, the generalized pressure P_a is the conjugate of V in the $(N, V, \mathbf{h}_0, T)$ ensemble.

2.3.2. Choice of $\boldsymbol{h}_0$. Since the unit cell retains its initial shape during $(N, V, \mathbf{h}_0, T)$ simulations, one can envision that the choice for the cell shape $\mathbf{h}_0$ may affect the obtained free energy profile and thus the predicted flexibility. To verify this statement, the cell shapes are chosen according to the following three approaches, and the obtained free energy profiles are labeled correspondingly:

(i) For $\text{TI}_{\mathbf{h}_0}^{\text{snap}}$, the cell shapes are determined as snapshots at the the required volume V from a prior $(N, P, \boldsymbol{\sigma}_a = \mathbf{0}, T)$ simulation, in which the cell shape could fluctuate freely.

(ii) For $\text{TI}_{\mathbf{h}_0}^{\text{mean}}$, the cell shapes are determined by the average cell shapes of a set of prior $(N, V, \boldsymbol{\sigma}_a = \mathbf{0}, T)$ simulations at the corresponding volume V of interest.

(iii) For $\text{TI}_{\mathbf{h}_0}^{\text{ipol}}$, the cell shapes are determined by an interpolation scheme between the two (meta)stable structures. For cubic materials, such as DUT-49(Cu), this interpolation scheme imposes cubic symmetry for all intermediate cell volumes $(\mathbf{h}_0(V) = \mathbf{1}, \forall V)$. For materials in which the (meta)stable states differ in symmetry, the interpolation scheme is more intricate (vide infra).

DOI: 10.1021/acs.jctc.7b01134
J. Chem. Theory Comput. XXXX, XXX, XXX−XXX

While we can use the standard formula for thermodynamic integration, eq 2.3, in each of the above techniques, the generalized expression in eq 2.8 can only be used if P_a in eq 2.9 can be calculated. For the schemes outlined above, this is only the case for the interpolation scheme. To show that eq 2.9 indeed yields a path-independent free energy difference between the two (meta)stable states, two interpolations are compared for MIL-53(Al): one linear and one quadratic. The linear interpolation scheme, ipol1, reads

$$\mathbf{h}^{\text{ipol1}}(\lambda) = \lambda \mathbf{h}_{\text{cp}} + (1 - \lambda)\mathbf{h}_{\text{lp}} \tag{2.10}$$

whereas the quadratic interpolation scheme, ipol2, is defined by

$$\mathbf{h}^{\text{ipol2}}(\lambda) = (\lambda + a\lambda(1 - \lambda))\mathbf{h}_{\text{cp}} + (1 - \lambda + a\lambda(1 - \lambda))\mathbf{h}_{\text{lp}} \tag{2.11}$$

where we chose $a = 1/20$.

Because each volume needs to be matched to a corresponding cell shape, $V \rightarrow \mathbf{h}_0(V)$, λ should be a bijective function of the volume V. This mapping is determined in both interpolation schemes via the self-consistent relation

$$\det(\mathbf{h}^{\text{ipol}}(\lambda(V))) = V \tag{2.12}$$

In both cases, $\lambda = 0$ corresponds to the lp cell matrix, whereas $\lambda = 1$ corresponds to the cp cell matrix. For intermediate volumes, both interpolation schemes yield different cell shapes: $\mathbf{h}^{\text{ipol1}}(\lambda(V)) \neq \mathbf{h}^{\text{ipol2}}(\lambda(V))$. The cell parameters as a function of the cell volume resulting from both interpolation schemes are discussed in section S1 of the Supporting Information.

To use eq 2.9, it is necessary to evaluate

$$\frac{\mathrm{d}\mathbf{F}}{\mathrm{d}V} = \frac{\mathrm{d}\mathbf{F}}{\mathrm{d}\lambda}\frac{\mathrm{d}\lambda}{\mathrm{d}V} \tag{2.13}$$

Here, $\mathrm{d}\mathbf{F}/\mathrm{d}\lambda$ is obtained by inserting either eq 2.10 or eq 2.11 in eq 2.5. The further evaluation of this expression is outlined in section S2 of the Supporting Information. For the ipol1 method and with the cp phase as reference state, the two factors in the expression above simplify to

$$\left.\frac{\mathrm{d}\mathbf{F}}{\mathrm{d}\lambda}\right|^{\text{ipol1}} = \mathbf{1} - \mathbf{h}_{\text{lp}}\mathbf{h}_{\text{cp}}^{-1} \tag{2.14}$$

$$\left.\frac{\mathrm{d}\lambda}{\mathrm{d}V}\right|^{\text{ipol1}} = \left[\frac{\mathrm{d}}{\mathrm{d}\lambda}\det(\lambda\mathbf{h}_{\text{cp}} + (1 - \lambda)\mathbf{h}_{\text{lp}})\right]^{-1} \tag{2.15}$$

which can be readily evaluated and inserted in eq 2.9 to define the generalized pressure P_a.

3. COMPUTATIONAL DETAILS

As outlined in the Methodology, all MD simulations in this work are carried out in either the $(N, P, \boldsymbol{\sigma}_a = \mathbf{0}, T)$, $(N, V, \boldsymbol{\sigma}_a = \mathbf{0}, T)$, or $(N, V, \mathbf{h}_0, T)$ ensemble, giving rise to free energy profiles labeled MTD, TI_{full}, and $\text{TI}_{\mathbf{h}_0}$, respectively. In these ensembles, the number of particles N is kept fixed and the temperature $T = 300$ K is controlled using a Nosé−Hoover chain consisting of three beads and with a relaxation time of 100 fs for MIL-53(Al) and 1000 fs for the larger DUT-49(Cu).[42−45] Where relevant, the pressure P and/or the anisotropic stress, $\boldsymbol{\sigma}_a$, are controlled to be zero using a Martyna−Tobias−Tuckerman−Klein (MTTK) barostat with a relaxation time of 1000 fs for MIL-53(Al) and 2000 fs for DUT-49(Cu).[46,47]

The energies and forces during the MD simulations were evaluated using earlier published force fields. For MIL-53(Al), the force field developed in ref 48 was employed, which is derived according to the QuickFF procedure.[49] For DUT-49(Cu), the force field developed in ref 23 was employed, which is derived within the MOF−FF framework[50] and supplemented with MM3 force field parameters for those parameters missing in MOF−FF.[51,52] We refer to refs 48 and 23 for the validation of both force fields. All MD simulations were carried out with the in-house-developed MD engine Yaff,[53] using a Verlet time step of 0.5 fs which ensures energy conservation. For computational efficiency, Yaff was interfaced with other MD engines. The long-range interactions in MIL-53(Al) were calculated with LAMMPS,[54] whereas DL_POLY[55] was used through the pydlpoly wrapper[50] to calculate both the short- and long-range interactions in DUT-49(Cu).

For MIL-53(Al), the conventional unit cell containing 76 atoms was doubled along the inorganic chain, forming a 1 × 2 × 1 supercell with 152 atoms. As shown in section S4 in the Supporting Information, the results presented here can be transferred to larger supercells. For DUT-49(Cu), the conventional unit cell containing 1728 atoms was used. VMD was used to visualize different snapshots of the simulations.[56]

For the MTD simulations in the $(N, P, \boldsymbol{\sigma}_a = \mathbf{0}, T)$ ensemble on MIL-53(Al), a set of 10 independent 2.2 ns simulations with different initial conditions are performed. During these simulations, subsequent Gaussian hills $U_b^{(i)}(V) = h_i \exp(-(V - V_i)^2/(2w_i^2))$ are centered on the volume V_i obtained by averaging the instantaneous volumes between the current and the previous metadynamics steps. These 2.2 ns simulations are divided into two stages. In the first 1.2 ns, the Gaussian hills have a height $h_i = 1$ kJ/mol and a width $w_i = 50$ Å^3 and are deposited every 0.6 ps. In the remaining 1 ns, the Gaussian hills have a smaller $h_i = 0.5$ kJ/mol and a smaller $w_i = 25$ Å^3 and are deposited every 1 ps.

To determine the (generalized) pressures for thermodynamic integration from either $(N, V, \boldsymbol{\sigma}_a = \mathbf{0}, T)$ or $(N, V, \mathbf{h}_0, T)$ simulations, the average (generalized) pressure is determined from 500 ps simulations (i) at 164 intermediate cell volumes, equally spaced between 720 and 1535 Å^3 for MIL-53(Al) and (ii) at 101 intermediate cell volumes, equally spaced between 40 000 and 100 000 Å^3 for DUT-49(Cu). To reduce unwanted noise in both the pressure and free energy equations of state, the obtained $P(V)$ data points are fitted to a polynomial before performing thermodynamic integration. Here, the order of the polynomial is determined to minimize the mean squared error (MSE) between the true and fitted pressure points. This MSE is calculated with a 5-fold cross-validation to correct for overfitting of the data.[57] For the free energy profile obtained using metadynamics simulations in the $(N, P, \boldsymbol{\sigma}_a = \mathbf{0}, T)$ ensemble, the degree of the free energy polynomial is chosen to be the same as that for the free energy polynomial obtained with the TI_{full} methodology, as they are virtually indistinguishable.

The variance on the reported volumes of the (meta)stable and transition states and their respective free energy differences are estimated using the bootstrap method with 100 samples for the TI methods.[57,58] For the MTD method, the variance is determined based on the 10 independent simulations.

4. RESULTS AND DISCUSSION

4.1. Free Energy Profiles Obtained by Integrating the Hydrostatic Pressure. To get a first estimate of the

DOI: 10.1021/acs.jctc.7b01134
J. Chem. Theory Comput. XXXX, XXX, XXX−XXX

inaccuracy $\Delta_{\mathbf{h}_0}F$ in free energy induced by neglecting proper cell shape sampling, free energy profiles have been constructed either from a $(N, V, \boldsymbol{\sigma}_a = \mathbf{0}, T)$ simulation (TI_{full}), in which the cell shape is sampled explicitly, or from a $(N, V, \mathbf{h}_0, T)$ simulation, in which the cell shape $\mathbf{h}_0$ was chosen by interpolation ($TI^{ipol}_{\mathbf{h}_0}$). Here, the free energy profiles are obtained by thermodynamic integration of the hydrostatic pressure P. In Figure 3, the resulting free energy equations of state are visualized for both MIL-53(Al) and DUT-49(Cu). In addition, the MIL-53(Al) free energy equation of state obtained by a metadynamics simulation in the $(N, P, \boldsymbol{\sigma}_a = \mathbf{0}, T)$ ensemble is also provided for comparison.

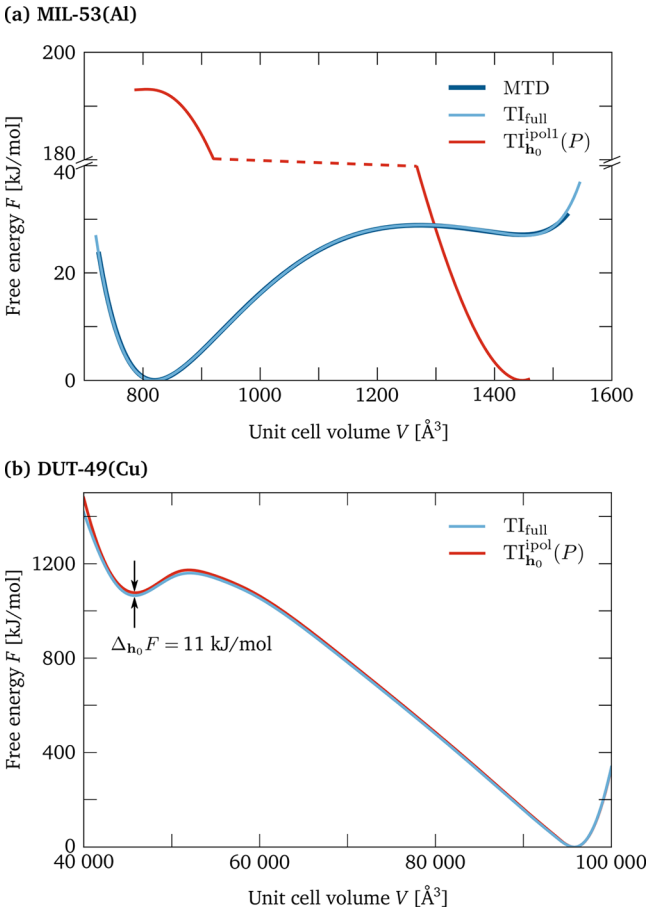

Figure 3. Free energy profiles F as a function of the cell volume V for (a) MIL-53(Al) and (b) DUT-49(Cu) at 300 K. For both materials, the profiles obtained with the TI_{full} (light blue) and the $TI^{ipol}_{\mathbf{h}_0}$ methods (red) are compared, based on thermodynamic integration of the hydrostatic pressure, P. For the MIL-53(Al), also the free energy profile obtained with metadynamics (dark blue) is provided. All profiles are shifted to be zero at their global minimum.

For the cubic DUT-49(Cu), shown in Figure 3b, the TI_{full} and $TI^{ipol}_{\mathbf{h}_0}$ free energy equations of state nearly coincide, showing a stable op minimum at a volume of ca. 95 700 Å^3 and a metastable cp minimum at a volume of ca. 45 800 Å^3, separated by a transition barrier of about 94 kJ/mol at a volume of ca. 52 500 Å^3. Table 2 lists the exact volumes of the (meta)stable states and the transition state, as well as their relative stability. Both methods give the same qualitative results for DUT-49(Cu), which agree well with the results obtained by Evans et al.[23] However, quantitatively, the relative stability of the cp phase with respect to the op phase differs by 11 ± 3 kJ/mol between the two methods. This difference is a consequence of neglecting cell shape sampling in the $TI^{ipol}_{\mathbf{h}_0}$ method: the cell shape is artificially kept fixed in the $TI^{ipol}_{\mathbf{h}_0}$ method while it can instantaneously deviate from perfect cubic symmetry in the reference TI_{full} method.

For MIL-53(Al), depicted in Figure 3a, the MTD and TI_{full} free energy equations of state coincide quantitatively (see also Table 3), indicating that both methods adequately sample the phase space associated with the cell shape and can be used as reference profiles including cell shape sampling, in line with earlier observations.[32] These profiles also coincide with earlier reported free energy equations of state.[19] In contrast, the $TI^{ipol1}_{\mathbf{h}_0}$ free energy equation of state obtained by thermodynamic integration of the hydrostatic pressure P clearly shows a different qualitative behavior, failing to reveal a stable cp minimum. While being conceptually the same method as the $TI^{ipol}_{\mathbf{h}_0}$ method for DUT-49(Cu), the symmetry of the two materials is different. For DUT-49(Cu), the op and cp phases share the cubic symmetry, for which $\mathbf{h}_0 = \mathbf{1}$. Therefore, the cell shape does not change upon straightforward interpolation, and the only difference between the TI_{full} and $TI^{ipol}_{\mathbf{h}_0}$ methods is cell shape sampling. Hence, we can immediately identify $\Delta_{\mathbf{h}_0}F$ for DUT-49(Cu) to be 11 ± 3 kJ/mol.

MIL-53(Al), in contrast, undergoes a change in symmetry from the orthorhombic *Pmma* to a monoclinic *P*2/*c* space group when undergoing a phase transition from the lp to the cp phase. Therefore, various interpolation schemes for the cell shape $\mathbf{h}_0$ at intermediate volumes can be chosen. As a result, one can envision that differences between the TI_{full} and $TI^{ipol1}_{\mathbf{h}_0}$ do not only stem from the lack of cell shape sampling in the latter method but also from the specific choice of fixed cell shape. In the following paragraph, we will indicate how this dependence can be mitigated for certain choices of this fixed cell shape.

4.2. Effect of the Choice of Fixed Cell Shape on the Free Energy Profiles. As hypothesized in the previous paragraph, the choice of fixed cell shape may affect the obtained free energy equations of state when integrating the hydrostatic pressure P. To verify this statement, the averaged hydrostatic internal pressure $P = \langle P_i \rangle$ during the $(N, V, \boldsymbol{\sigma}_a = \mathbf{0},$

Table 2. (Meta)stable and Transition State Volumes of DUT-49(Cu) and Their Relative Stability at 300 K As Predicted from the Methods in Figure 3b, Using the Hydrostatic Pressure, P

method	V_{cp} (Å^3)	V_{tr} (Å^3)	V_{op} (Å^3)	$F_{cp} - F_{op}$ (kJ/mol)	$F_{tr} - F_{cp}$ (kJ/mol)
TI_{full}	45 803(16)	52 536(52)	95 702(21)	1065(2)	94(2)
$TI^{ipol}_{\mathbf{h}_0}$	45 765(14)	52 517(38)	95 755(21)	1076(2)	94(2)
$TI^{ipol}_{\mathbf{h}_0} - TI_{full}$	−38(21)	−19(64)	53(30)	11(3)	0(3)

DOI: 10.1021/acs.jctc.7b01134
J. Chem. Theory Comput. XXXX, XXX, XXX−XXX

Table 3. (Meta)stable and Transition State Volumes of MIL-53(Al) and Their Relative Stability at 300 K As Predicted from the Methods in Figure 5

method	V_{cp} (Å^3)	V_{barr} (Å^3)	V_{lp} (Å^3)	$F_{lp} - F_{cp}$ (kJ/mol)	$F_{barr} - F_{cp}$ (kJ/mol)
MTD	820.24(10)	1272.3(5)	1446.9(5)	27.13(2)	28.90(2)
TI_{full}	819.1(5)	1276(6)	1451(2)	27.00(6)	28.96(7)
$TI_{h_0}^{ipol1}$	820(1)		1435(1)	13.135(4)	
$TI_{h_0}^{ipol2}$	820(1)		1435(1)	13.165(6)	
$TI_{h_0}^{ipol1} - TI_{full}$	1(1)		−16(2)	−13.87(6)	
$TI_{h_0}^{ipol2} - TI_{full}$	1(1)		−16(2)	−13.84(6)	

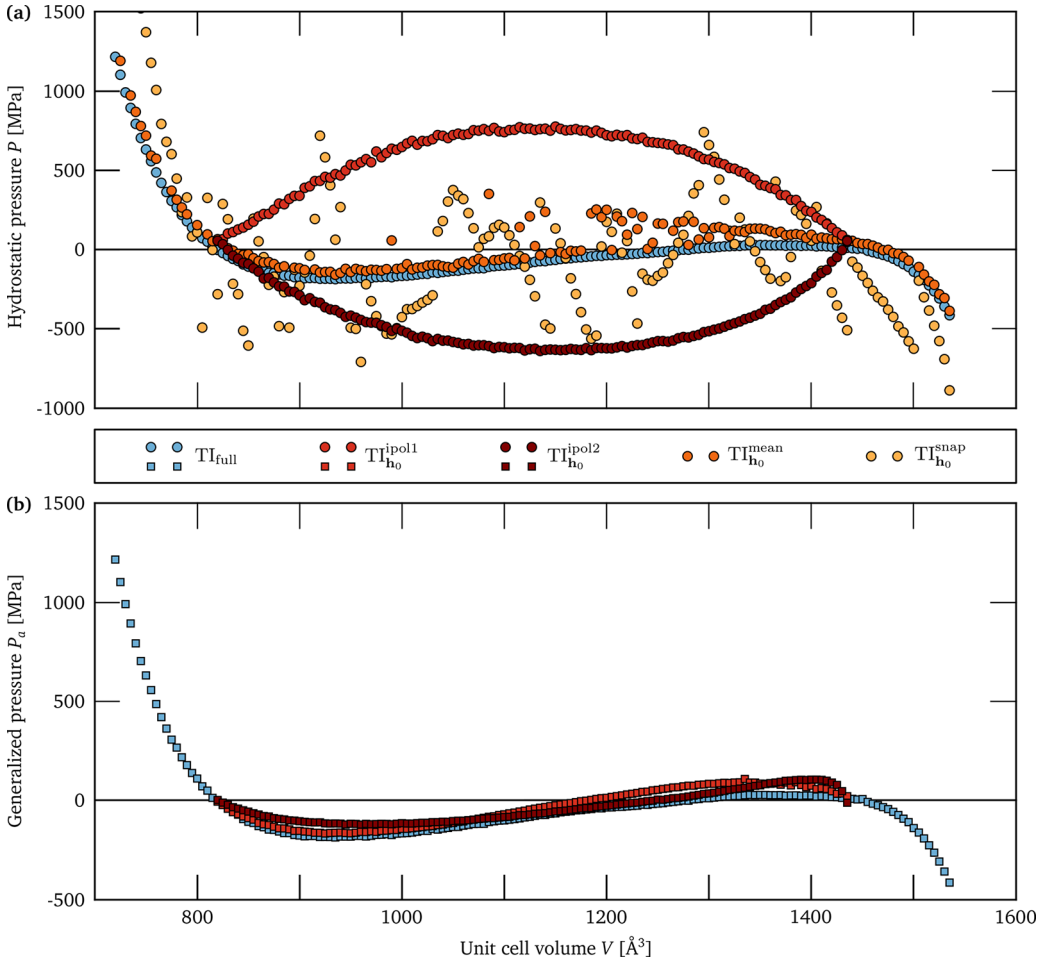

Figure 4. (a) Hydrostatic pressure P and (b) generalized pressure, P_a, profiles as a function of the cell volume V for MIL-53(Al) at 300 K obtained within the (N, V, $\boldsymbol{\sigma}_a = \mathbf{0}$, T) ensemble (light blue) and the (N, V, $\mathbf{h}_0$, T) ensemble with four choices of the fixed cell shape $\mathbf{h}_0$ (red shades).

T) simulations (TI_{full}) or (N, V, $\mathbf{h}_0$, T) simulations (TI_{h_0}) is calculated as a function of the unit cell volume for MIL-53(Al) and depicted in Figure 4a. As can be observed from this figure, the hydrostatic pressure P does indeed vary between the four different TI_{h_0} methods (Table 1) and therefore depends on the choice of fixed cell shape. Moreover, the resulting TI_{h_0} pressure profiles deviate from the profile obtained with the TI_{full} method, which in turn leads to different free energy equations of state through eq 2.3.

Figure 4a further clarifies the dependence of this hydrostatic pressure on the choice of the cell shape $\mathbf{h}_0$ for the simulations with fixed unit cell shape. The $TI_{h_0}^{snap}$ method, in which the cell shapes are obtained as snapshots of a preceding constant-pressure simulation, shows a randomly fluctuating pressure profile. For the $TI_{h_0}^{mean}$ method, in which the cell shapes are chosen as the average of preceding (N, V, $\boldsymbol{\sigma}_a = \mathbf{0}$, T) simulations, the behavior is already much smoother. However, large deviations in the pressure are still present close to the transition volume of about 1270 Å^3. Finally, the two interpolation methods give a smooth pressure equation of state but fail to correctly predict the two (meta)stable phases, as was already apparent in Figure 3a for the first interpolation method. Indeed, to correctly predict the relative stability in MIL-53(Al) at 300 K and 0 MPa, the pressure equation of state should cross the horizontal at P = 0 MPa three times: once for each (meta)stable phase, and once for the transition state. For the two pressure profiles obtained by interpolation, only two

DOI: 10.1021/acs.jctc.7b01134
J. Chem. Theory Comput. XXXX, XXX, XXX−XXX

crossings are present, leading to one stable state and one transition state, as also observed in Figure 3a.

To further investigate the difference in the hydrostatic pressure P, all elements of the average internal stress tensor, $\langle \boldsymbol{\sigma}_i \rangle$, have been determined (see section S3 of the Supporting Information). In contrast to simulations in the $(N, V, \boldsymbol{\sigma}_a = \mathbf{0}, T)$ ensemble, in which the cell shape fluctuates in such a way as to lead to a vanishing average deviatoric stress, $\boldsymbol{\sigma}_a = \mathbf{0}$, the fixed cell shape in the $(N, V, \mathbf{h}_0, T)$ ensemble generally leads to nonvanishing average deviatoric stresses, $\boldsymbol{\sigma}_a \neq \mathbf{0}$. As a result, the hydrostatic pressure, P alone no longer conveys sufficient information to describe the current stress state of the system. Therefore, the hydrostatic pressure and the volume are no longer thermodynamically conjugate variables, and one has to rely on the second Piola−Kirchhoff tensor, $\mathbf{S}$, and the Lagrangian strain, $\boldsymbol{\eta}$. As outlined in section 2.3 of the Methodology, the relevant free energy equation of state in the $(N, V, \mathbf{h}_0, T)$ ensemble is then obtained by integrating the generalized pressure P_a, as given in eqs 2.8 and 2.9. While this is the most general procedure, specific cases exist where the average deviatoric stress does vanish, despite keeping the unit cell shape fixed. This is for instance the case when the unit cell is cubic through the whole volume range of interest, such as for DUT-49(Cu), so that deviatoric stresses disappear because of the symmetry of the unit cell (see section S2 in the Supporting Information).

In Figure 4b, this generalized pressure P_a is plotted as a function of the volume for the interpolation methods and the $\mathrm{TI}_{\mathrm{full}}$ method, for which $P_a = P$. The three generalized pressure equations of state now yield the same qualitative behavior, with two stable branches (for which $\partial P/\partial V < 0$) and one unstable branch (for which $\partial P/\partial V > 0$), correctly identifying the (meta)stable cp and lp states as well as an unstable transition state. Because the two interpolation schemes only coincide in the end points, corresponding to the cp and lp states, only the free energy difference between these two end points can be contrasted. Since, in general, $\mathbf{h}^{\mathrm{ipol1}}(\lambda(V)) \neq \mathbf{h}^{\mathrm{ipol2}}(\lambda(V))$, the free energy difference between any two intermediate points depends on the interpolation scheme and cannot be compared. As there is no continuous path of the cell shape as a function of the cell volume for the $\mathrm{TI}^{\mathrm{snap}}_{\mathbf{h}_0}$ and $\mathrm{TI}^{\mathrm{mean}}_{\mathbf{h}_0}$ methods (see section S1 of the Supporting Information), no generalized pressure P_a could be calculated through eq 2.9, and these methods will not be discussed further.

The three methods for which the generalized P_a was calculated are visualized in Figure 5. Despite having a different choice of considered cell shape at intermediate volumes, and thus $\mathbf{h}^{\mathrm{ipol1}}(\lambda(V)) \neq \mathbf{h}^{\mathrm{ipol2}}(\lambda(V))$, the free energy profiles obtained with the two interpolation methods predict the same free energy difference between the cp and metastable lp phase. This indicates that the generalized pressure P_a can be used to uniquely define the free energy difference between two (meta)stable states in an ensemble in which the cell shape is kept fixed, given that a continuous path $V \rightarrow \mathbf{h}_0(V)$ between the (meta)stable states is defined such that eq 2.8 can be calculated. Note, however, that only the free energy difference between the two (meta)stable states, the end points of the interpolation, can be calculated. The free energy difference between any two other points on the profile, including the transition state, depends on the specific interpolation scheme and cannot be directly compared, highlighting an important drawback of simulating in the $(N, V, \mathbf{h}_0, T)$ ensemble.

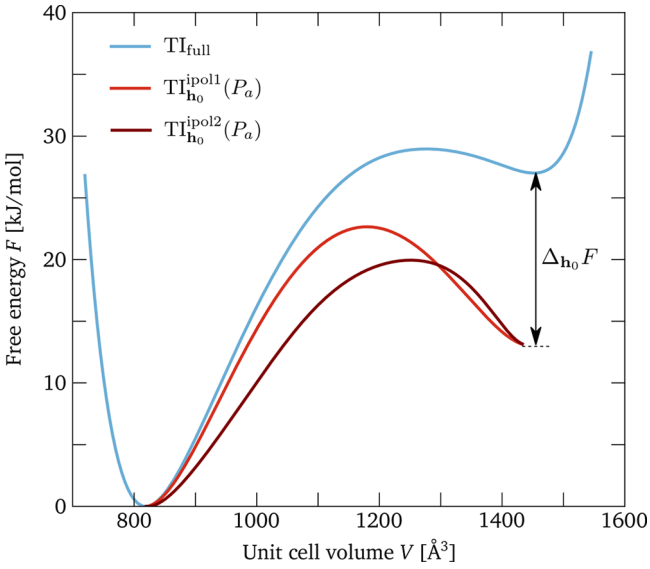

Figure 5. Free energy profiles F as a function of the unit cell volume V for MIL-53(Al) at 300 K obtained by thermodynamic integration of the hydrostatic pressure P in the $(N, V, \boldsymbol{\sigma}_a = \mathbf{0}, T)$ ensemble ($\mathrm{TI}_{\mathrm{full}}$, light blue) or the generalized pressure P_a in the $(N, V, \mathbf{h}_0, T)$ ensemble with interpolated cell shapes ($\mathrm{TI}^{\mathrm{ipol1}}_{\mathbf{h}_0}$ and $\mathrm{TI}^{\mathrm{ipol2}}_{\mathbf{h}_0}$, red).

As indicated in Table 3, in which the volumes of the (meta)stable and transition states as well as their relative stability are given, both methods predict that the cp state is about 13 kJ/mol more stable than the (meta)stable lp state at 300 K, in contrast to the 27 kJ/mol obtained when fully taking cell shape fluctuations into account. Hence, the lack of cell shape sampling results in an inaccuracy in free energy amounting to $\Delta_{\mathbf{h}_0} F = 13.84 \pm 0.06$ kJ/mol for MIL-53(Al).

4.3. Enthalpic and Entropic Contributions of Cell Shape Sampling. In the previous paragraphs, we quantified the inaccuracy $\Delta_{\mathbf{h}_0} F$ introduced by neglecting proper cell shape sampling, amounting to 13.84 ± 0.06 kJ/mol for MIL-53(Al) and 11 ± 3 kJ/mol for DUT-49(Cu). This discrepancy is of the same order of magnitude for the two materials despite their strongly differing unit cell and the strongly different relative stability of the (meta)stable phases. To get further insight into the origin of this discrepancy, the free energy equations of state reported in Figure 3b for DUT-49(Cu) and Figure 5 for MIL-53(Al) have been subdivided into their enthalpic and entropic contributions, according to the relation $F = E - TS$. The resulting relative energy and relative entropy equations of state are reported in Figure 6 and Figure 7 for MIL-53(Al) and DUT-49(Cu), respectively. The extracted differences in free energy, energy, and entropy between the two (meta)stable states are reported in Table 4 and Table 5.

For MIL-53(Al), the energy difference ΔE between the lp and cp states amounts to about 41 kJ/mol, independent of whether the cell shape is kept fixed during the simulation. However, the entropy difference $T\Delta S$ between these two (meta)stable states does depend on whether the cell shape is sampled. The relative entropy of the lp state increases when fixing the cell shape. This increase in relative entropy emphasizes a larger cell flexibility for the cp state with respect to the lp state. When fully accounting for cell shape sampling in the $\mathrm{TI}_{\mathrm{full}}$ method, this entropy difference amounts to about 14 kJ/mol, while this value increases to about 28 kJ/mol when cell shape sampling is neglected in the $\mathrm{TI}_{\mathbf{h}_0}$ method. The inaccuracy

DOI: 10.1021/acs.jctc.7b01134
J. Chem. Theory Comput. XXXX, XXX, XXX−XXX

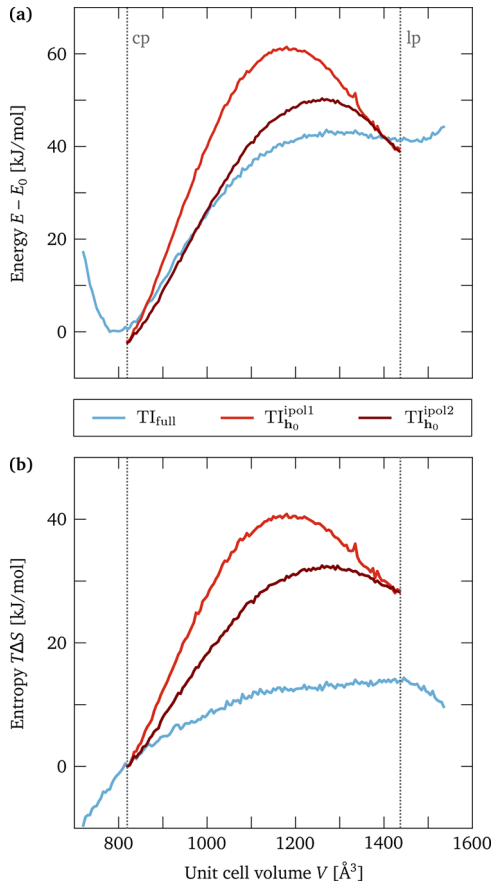

Figure 6. (a) Relative energy profile, ΔE, and (b) relative entropy profile, $T\Delta S$, as a function of the unit cell volume V for MIL-53(Al) at 300 K as obtained with the TI_{full}, $TI^{ipol1}_{h_0}$, and $TI^{ipol2}_{h_0}$ methods. The energies are shifted uniformly over E_0 = −24 002 kJ/mol for all methods, while the entropies are shifted for each method separately to yield 0 at the cp volume.

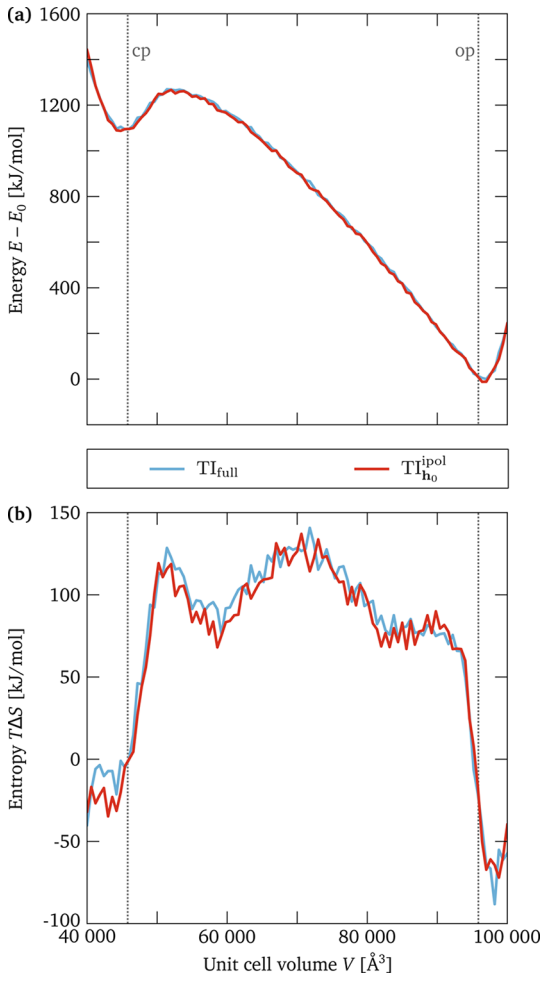

Figure 7. (a) Relative energy profile, ΔE, and (b) relative entropy profile, $T\Delta S$, as a function of the unit cell volume V for DUT-49(Cu) at 300 K as obtained with the TI_{full} and $TI^{ipol}_{h_0}$ methods. The energies are shifted over E_0 = −28 401 kJ/mol for all methods, while the entropies are shifted for each method separately to yield 0 at the cp volume.

in free energy difference $\Delta_{h_0}F$ = 13.84 ± 0.06 kJ/mol for MIL-53(Al) can hence be completely explained by entropic contributions at 300 K.

Likewise, for DUT-49(Cu), the inaccuracy in the energy difference ΔE between the op and cp states when neglecting cell shape sampling only amounts to about 3 kJ/mol, which remains within the imprecision due to the finite simulation time. In contrast, the inaccuracy in entropy difference $T\Delta S$ between these two states amounts to 8 kJ/mol, which largely accounts for the inaccuracy in free energy difference $\Delta_{h_0}F$ = 11 ± 3 kJ/mol observed for DUT-49(Cu) at 300 K.

5. CONCLUSIONS

In the continuing quest to find flexible MOFs exhibiting outstanding behavior in a range of applications, a large variety of hypothetical MOFs have been put forward. However, a computational screening to identify outstanding MOFs requires reliable knowledge on the triggers for their flexibility, allowing one to rationalize their behavior before their actual synthesis. Recently, the free energy equations of state were determined to be the most reliable theoretical method to extract information on the relative stability of the various (meta)stable phases of the material, as well as on the conditions of temperature and pressure needed to induce a phase transition.[59] However, when generating these equations of state, the unit cell shape is not always sampled adequately. In this work, we quantified the inaccuracy in predicted free energy difference between the metastable states of MIL-53(Al) and DUT-49(Cu), two representative flexible MOFs, when not properly taking cell shape fluctuations into account.

Table 4. Difference in Free Energy, ΔF, Energy, ΔE, and Entropy, $T\Delta S$, between the lp and cp Phases of MIL-53(Al) at 300 K As Predicted from the TI Methods Depicted in Figure 5

method	ΔF (kJ/mol)	ΔE (kJ/mol)	$T\Delta S$ (kJ/mol)
TI_{full}	27.00	40.86	13.84
$TI^{ipol1}_{h_0}$	13.14	41.58	28.49
$TI^{ipol2}_{h_0}$	13.17	41.29	28.23
$TI^{ipol1}_{h_0}$ − TI_{full}	−13.87	0.72	14.65
$TI^{ipol2}_{h_0}$ − TI_{full}	−13.84	0.43	14.39

First, we demonstrated that thermodynamic integration of the hydrostatic pressure, P, only gives a well-defined free energy equation of state when fully accounting for cell shape sampling during the simulation. In contrast, thermodynamic integration

DOI: 10.1021/acs.jctc.7b01134
J. Chem. Theory Comput. XXXX, XXX, XXX−XXX

Table 5. Difference in Free Energy, ΔF, Energy, ΔE, and Entropy, $T\Delta S$, between the op and cp Phases of DUT-49(Cu) at 300 K As Predicted from the TI Methods Depicted in Figure 3b

method	ΔF (kJ/mol)	ΔE (kJ/mol)	$T\Delta S$ (kJ/mol)
TI_{full}	1065	1082	17
$TI_{h_0}^{ipol}$	1076	1085	9
$TI_{h_0}^{ipol} - TI_{full}$	11	3	−8

of the hydrostatic pressure P when neglecting cell shape sampling yields free energy profiles which are not reliable. They fail to predict the two metastable states in MIL-53(Al) since the deviatoric stress does not vanish ($\boldsymbol{\sigma}_a \neq \mathbf{0}$). Moreover, the obtained hydrostatic pressure and hence relative stability of the metastable phases depend on the choice of the cell shape. For DUT-49(Cu), the deviatoric stress does vanish even when fixing the cell shape, as the cubic symmetry is conserved during the phase transformation between the two metastable states. As a result, the free energy profile obtained when fixing the cell shape qualitatively predicts the presence of the two metastable states. However, a quantitative difference in free energy difference between the DUT-49(Cu) metastable phases was observed when neglecting cell shape sampling, which amounts to $\Delta_{h_0}F = 11 \pm 3$ kJ/mol.

Second, an extension to the thermodynamic integration protocol was proposed and its validity was assessed on MIL-53(Al). If a continuous path of the cell shape as a function of the volume exists between the two metastable states, as could be established in the interpolation method, a generalized pressure, P_a, can be defined which explicitly takes the nonvanishing internal deviatoric stresses into account. Thermodynamic integration of this generalized pressure yields a smooth free energy equation of state. Moreover, the predicted difference in free energy between the MIL-53(Al) lp and cp states does not depend on the intermediate volumes, hence yielding a unique and well-defined free energy difference, $F_{lp} - F_{cp}$, between these two metastable states. The inaccuracy in free energy difference because of the lack of cell shape sampling, $\Delta_{h_0}F$, amounts to 13.83 ± 0.06 kJ/mol for this material.

Third, the inaccuracy in free energy difference, $\Delta_{h_0}F$, consists of an enthalpic and an entropic contribution. For the two materials under study in this work, MIL-53(Al) and DUT-49(Cu), we observed that the inaccuracy as a result of neglecting cell shape sampling is mainly due to the entropy at 300 K, which is not correctly described when the cell shape is constrained.

In conclusion, we demonstrated in this work that neglecting proper sampling of the phase space associated with the unit cell shape yields erroneous predictions of the relative stability of the metastable phases in flexible materials. For a general flexible MOF, this mismatch is both due to the constraint of a fixed cell shape, as this generally induces deviatoric stresses, and due to the reduced sampling of the phase space. The former issue disappears when defining a generalized P_a if the intermediate cell shapes are chosen according to an interpolation scheme between the metastable phases. In contrast, the mismatch due to the reduced sampling inherently leads to an incorrect entropy difference between the metastable phases. We successfully quantified this inaccuracy in free energy, $\Delta_{h_0}F$, amounting to about 10−15 kJ/mol for both MIL-53(Al) and DUT-49(Cu). While this inaccuracy does not significantly alter the predicted free energy profile for DUT-49(Cu), it is important to reliably predict flexibility in MIL-53(Al). Given that the lp phase in MIL-53(Al) is only 27 kJ/mol less stable than the cp phase, one should be careful in selecting the correct ensemble, ensuring explicit cell shape sampling when generating free energy profiles for flexible MOFs.

■ ASSOCIATED CONTENT

Supporting Information

The Supporting Information is available free of charge on the ACS Publications website at DOI: 10.1021/acs.jctc.7b01134.

Visualization of the cell parameters as a function of the volume for the two interpolation schemes of MIL-53(Al), derivation of the expression for the generalized pressure P_a and simplification for cubic cells, average internal stress tensor for the different methods, and influence of the supercell size on the reported pressure equations of state (PDF)

■ AUTHOR INFORMATION

Corresponding Author

*E-mail: An.Ghysels@UGent.be.

ORCID

Sven M. J. Rogge: 0000-0003-4493-5708
Ruben Demuynck: 0000-0003-3475-8808
Veronique Van Speybroeck: 0000-0003-2206-178X
An Ghysels: 0000-0003-0015-2605

Author Contributions

†S.M.J.R. and S.C. contributed equally to this work.

Funding

This work is supported by the Fund for Scientific Research Flanders (FWO), the Research Board of Ghent University (BOF), and BELSPO in the frame of IAP/7/05.

Notes

The authors declare no competing financial interest.

■ ACKNOWLEDGMENTS

Computational resources (Stevin Supercomputer Infrastructure) and services were provided by Ghent University. We thank Steven Vandenbrande, Johannes Dürholt, and Jack D. Evans for insightful discussions on the topic.

■ REFERENCES

(1) Li, H.; Eddaoudi, M.; O'Keeffe, M.; Yaghi, O. M. Design and Synthesis of an Exceptionally Stable and Highly Porous Metal-Organic Framework. *Nature* **1999**, *402*, 276−279.

(2) Férey, G. Microporous Solids: From Organically Templated Inorganic Skeletons to Hybrid Frameworks···Ecumenism in Chemistry. *Chem. Mater.* **2001**, *13*, 3084−3098.

(3) Kitagawa, S.; Kitaura, R.; Noro, S.-i. Functional Porous Coordination Polymers. *Angew. Chem., Int. Ed.* **2004**, *43*, 2334−2375.

(4) Rogge, S. M. J.; Bavykina, A.; Hajek, J.; Garcia, H.; Olivos-Suarez, A. I.; Sepúlveda-Escribano, A.; Vimont, A.; Clet, G.; Bazin, P.; Kapteijn, F.; Daturi, M.; Ramos-Fernandez, E. V.; Llabrés i Xamena, F. X.; Van Speybroeck, V.; Gascon, J. Metal-Organic and Covalent Organic Frameworks as Single-Site Catalysts. *Chem. Soc. Rev.* **2017**, *46*, 3134−3184.

(5) Horcajada, P.; Gref, R.; Baati, T.; Allan, P. K.; Maurin, G.; Couvreur, P.; Férey, G.; Morris, R. E.; Serre, C. Metal-Organic Frameworks in Biomedicine. *Chem. Rev.* **2012**, *112*, 1232−1268.

DOI: 10.1021/acs.jctc.7b01134
J. Chem. Theory Comput. XXXX, XXX, XXX−XXX

(6) Li, J.-R.; Kuppler, R. J.; Zhou, H.-C. Selective Gas Adsorption and Separation in Metal-Organic Frameworks. *Chem. Soc. Rev.* **2009**, *38*, 1477−1504.
(7) Watanabe, T.; Sholl, D. S. Accelerating Applications of Metal-Organic Frameworks for Gas Adsorption and Separation by Computational Screening of Materials. *Langmuir* **2012**, *28*, 14114−14128.
(8) Schneemann, A.; Bon, V.; Schwedler, I.; Senkovska, I.; Kaskel, S.; Fischer, R. A. Flexible Metal-Organic Frameworks. *Chem. Soc. Rev.* **2014**, *43*, 6062−6096.
(9) Coudert, F.-X. Responsive Metal-Organic Frameworks and Framework Materials: Under Pressure, Taking the Heat, in the Spotlight, with Friends. *Chem. Mater.* **2015**, *27*, 1905−1916.
(10) Férey, G.; Serre, C. Large Breathing Effects in Three-Dimensional Porous Hybrid Matter: Facts, Analyses, Rules and Consequences. *Chem. Soc. Rev.* **2009**, *38*, 1380−1399.
(11) Nouar, F.; Devic, T.; Chevreau, H.; Guillou, N.; Gibson, E.; Clet, G.; Daturi, M.; Vimont, A.; Grenèche, J. M.; Breeze, M. I.; Walton, R. I.; Llewellyn, P. L.; Serre, C. Tuning the Breathing Behaviour of MIL-53(Al) by Cation Mixing. *Chem. Commun.* **2012**, *48*, 10237−10239.
(12) Sarkisov, L.; Martin, R. L.; Haranczyk, M.; Smit, B. On the Flexibility of Metal-Organic Frameworks. *J. Am. Chem. Soc.* **2014**, *136*, 2228−2231.
(13) Nanthamathee, C.; Ling, S.; Slater, B.; Attfield, M. P. Contradistinct Thermoresponsive Behavior of Isostructural MIL-53 Type Metal-Organic Frameworks by Modifying the Framework Inorganic Anion. *Chem. Mater.* **2015**, *27*, 85−95.
(14) Loiseau, T.; Serre, C.; Huguenard, C.; Fink, G.; Taulelle, F.; Henry, M.; Bataille, T.; Férey, G. A Rationale for the Large Breathing of the Porous Aluminum Terephthalate (MIL-53) upon Hydration. *Chem. - Eur. J.* **2004**, *10*, 1373−1382.
(15) Liu, Y.; Her, J.-H.; Dailly, A.; Ramirez-Cuesta, A. J.; Neumann, D. A.; Brown, C. M. Reversible Structural Transition in MIL-53 with Large Temperature Hysteresis. *J. Am. Chem. Soc.* **2008**, *130*, 11813−11818.
(16) Beurroies, I.; Boulhout, M.; Llewellyn, P. L.; Kuchta, B.; Férey, G.; Serre, C.; Denoyel, R. Using Pressure to Provoke the Structural Transition of Metal-Organic Frameworks. *Angew. Chem., Int. Ed.* **2010**, *49*, 7526−7529.
(17) Yot, P. G.; Boudene, Z.; Macia, J.; Granier, D.; Vanduyfhuys, L.; Verstraelen, T.; Van Speybroeck, V.; Devic, T.; Serre, C.; Férey, G.; Stock, N.; Maurin, G. Metal-Organic Frameworks as Potential Shock Absorbers: Case of the Highly Flexible MIL-53(Al). *Chem. Commun.* **2014**, *50*, 9462−9464.
(18) Serre, C.; Bourrelly, S.; Vimont, A.; Ramsahye, N. A.; Maurin, G.; Llewellyn, P. L.; Daturi, M.; Filinchuk, Y.; Leynaud, O.; Barnes, P.; Férey, G. An Explanation for the Very Large Breathing Effect of a Metal-Organic Framework during CO_2 Adsorption. *Adv. Mater.* **2007**, *19*, 2246−2251.
(19) Rogge, S. M. J.; Vanduyfhuys, L.; Ghysels, A.; Waroquier, M.; Verstraelen, T.; Maurin, G.; Van Speybroeck, V. A Comparison of Barostats for the Mechanical Characterization of Metal-Organic Frameworks. *J. Chem. Theory Comput.* **2015**, *11*, 5583−5597.
(20) Stoeck, U.; Krause, S.; Bon, V.; Senkovska, I.; Kaskel, S. A Highly Porous Metal-Organic Framework, Constructed From a Cuboctahedral Super-Molecular Building Block, with Exceptionally High Methane Uptake. *Chem. Commun.* **2012**, *48*, 10841−10843.
(21) Krause, S.; Bon, V.; Senkovska, I.; Stoeck, U.; Wallacher, D.; Többens, D. M.; Zander, S.; Pillai, R. S.; Maurin, G.; Coudert, F.-X.; Kaskel, S. A Pressure-Amplifying Framework Material with Negative Gas Adsorption Transitions. *Nature* **2016**, *532*, 348−352.
(22) Schaber, J.; Krause, S.; Paasch, S.; Senkovska, I.; Bon, V.; Többens, D. M.; Wallacher, D.; Kaskel, S.; Brunner, E. In Situ Monitoring of Unique Switching Transitions in the Pressure-Amplifying Flexible Framework Material DUT-49 by High-Pressure ^{129}Xe NMR Spectroscopy. *J. Phys. Chem. C* **2017**, *121*, 5195−5200.
(23) Evans, J. D.; Bocquet, L.; Coudert, F.-X. Origins of Negative Gas Adsorption. *Chem.* **2016**, *1*, 873−886.
(24) Coudert, F.-X.; Fuchs, A. H. Computational Characterization and Prediction of Metal-Organic Framework Properties. *Coord. Chem. Rev.* **2016**, *307*, 211−236.
(25) Coudert, F.-X.; Jeffroy, M.; Fuchs, A. H.; Boutin, A.; Mellot-Draznieks, C. Thermodynamics of Guest-Induced Structural Transitions in Hybrid Organic-Inorganic Frameworks. *J. Am. Chem. Soc.* **2008**, *130*, 14294−14302.
(26) Bousquet, D.; Coudert, F.-X.; Boutin, A. Free Energy Landscapes for the Thermodynamic Understanding of Adsorption-Induced Deformations and Structural Transitions in Porous Materials. *J. Chem. Phys.* **2012**, *137*, 044118.
(27) Ghysels, A.; Vanduyfhuys, L.; Vandichel, M.; Waroquier, M.; Van Speybroeck, V.; Smit, B. On the Thermodynamics of Framework Breathing: A Free Energy Model for Gas Adsorption in MIL-53. *J. Phys. Chem. C* **2013**, *117*, 11540−11554.
(28) Coudert, F.-X.; Boutin, A.; Fuchs, A. H. A Thermodynamic Description of the Adsorption-Induced Structural Transitions in Flexible MIL-53 Metal-Organic Framework. *Mol. Phys.* **2014**, *112*, 1257−1261.
(29) Rogge, S. M. J.; Wieme, J.; Vanduyfhuys, L.; Vandenbrande, S.; Maurin, G.; Verstraelen, T.; Waroquier, M.; Van Speybroeck, V. Thermodynamic Insight in the High-Pressure Behavior of UiO-66: Effect of Linker Defects and Linker Expansion. *Chem. Mater.* **2016**, *28*, 5721−5732.
(30) Vanduyfhuys, L.; Rogge, S. M. J.; Wieme, J.; Vandenbrande, S.; Maurin, G.; Waroquier, M.; Van Speybroeck, V. Thermodynamic Insight into Stimuli-Responsive Behaviour of Soft Porous Crystals. *Nat. Commun.* **2018**, *9*, 204.
(31) Wieme, J.; Vanduyfhuys, L.; Rogge, S. M. J.; Waroquier, M.; Van Speybroeck, V. Exploring the Flexibility of MIL-47(V)-Type Materials Using Force Field Molecular Dynamics Simulations. *J. Phys. Chem. C* **2016**, *120*, 14934−14947.
(32) Demuynck, R.; Rogge, S. M. J.; Vanduyfhuys, L.; Wieme, J.; Waroquier, M.; Van Speybroeck, V. Efficient Construction of Free Energy Profiles of Breathing Metal-Organic Frameworks Using Advanced Molecular Dynamics Simulations. *J. Chem. Theory Comput.* **2017**, *13*, 5861−5873.
(33) Kirkwood, J. G. Statistical Mechanics of Fluid Mixtures. *J. Chem. Phys.* **1935**, *3*, 300−313.
(34) Torrie, G. M.; Valleau, J. P. Nonphysical Sampling Distributions in Monte Carlo Free-Energy Estimation - Umbrella Sampling. *J. Comput. Phys.* **1977**, *23*, 187−199.
(35) Laio, A.; Parrinello, M. Escaping Free-Energy Minima. *Proc. Natl. Acad. Sci. U. S. A.* **2002**, *99*, 12562−12566.
(36) Cheatham, T. E., III; Miller, J. L.; Fox, T.; Darden, T. A.; Kollman, P. A. Molecular Dynamics Simulations on Solvated Biomolecular Systems: The Particle Mesh Ewald Method Leads to Stable Trajectories of DNA, RNA, and Proteins. *J. Am. Chem. Soc.* **1995**, *117*, 4193−4194.
(37) Frenkel, D.; Smit, B. *Understanding Molecular Simulation: From Algorithms to Applications*; Academic Press: New York, 2002.
(38) Basconi, J. E.; Shirts, M. R. Effects of Temperature Control Algorithms on Transport Properties and Kinetics in Molecular Dynamics Simulations. *J. Chem. Theory Comput.* **2013**, *9*, 2887−2899.
(39) Haigis, V.; Coudert, F.-X.; Vuilleumier, R.; Boutin, A.; Fuchs, A. H. Hydrothermal Breakdown of Flexible Metal-Organic Frameworks: A Study by First-Principles Molecular Dynamics. *J. Phys. Chem. Lett.* **2015**, *6*, 4365−4370.
(40) Tadmor, E. B.; Miller, R. E. *Modeling Materials: Continuum, Atomistic and Multiscale Techniques*; Cambridge University Press: New York, 2011.
(41) Wallace, D. C. Thermoelastic Theory of Stressed Crystals and Higher-Order Elastic Constants. *Solid State Phys.* **1970**, *25*, 301−404.
(42) Nosé, S. A Molecular Dynamics Method for Simulations in the Canonical Ensemble. *Mol. Phys.* **1984**, *52*, 255−268.
(43) Nosé, S. A Unified Formulation of the Constant Temperature Molecular Dynamics Methods. *J. Chem. Phys.* **1984**, *81*, 511−519.
(44) Hoover, W. G. Canonical Dynamics: Equilibrium Phase-Space Distributions. *Phys. Rev. A: At., Mol., Opt. Phys.* **1985**, *31*, 1695−1697.

DOI: 10.1021/acs.jctc.7b01134
J. Chem. Theory Comput. XXXX, XXX, XXX−XXX

(45) Martyna, G. J.; Klein, M. L.; Tuckerman, M. E. Nosé-Hoover Chains: The Canonical Ensemble via Continuous Dynamics. *J. Chem. Phys.* **1992**, *97*, 2635−2643.
(46) Martyna, G. J.; Tobias, D. J.; Klein, M. L. Constant Pressure Molecular Dynamics Algorithms. *J. Chem. Phys.* **1994**, *101*, 4177−4189.
(47) Martyna, G. J.; Tuckerman, M. E.; Tobias, D. J.; Klein, M. L. Explicit Reversible Integrators for Extended Systems Dynamics. *Mol. Phys.* **1996**, *87*, 1117−1157.
(48) Vanduyfhuys, L.; Verstraelen, T.; Vandichel, M.; Waroquier, M.; Van Speybroeck, V. Ab Initio Parametrized Force Field for the Flexible Metal-Organic Framework MIL-53(Al). *J. Chem. Theory Comput.* **2012**, *8*, 3217−3231.
(49) Vanduyfhuys, L.; Vandenbrande, S.; Verstraelen, T.; Schmid, R.; Waroquier, M.; Van Speybroeck, V. QuickFF: A Program for a Quick and Easy Derivation of Force Fields for Metal-Organic Frameworks from Ab Initio Input. *J. Comput. Chem.* **2015**, *36*, 1015−1027.
(50) Bureekaew, S.; Amirjalayer, S.; Tafipolsky, M.; Spickermann, C.; Roy, T. K.; Schmid, R. MOF-FF - A Flexible First-Principles Derived Force Field for Metal-Organic Frameworks. *Phys. Status Solidi B* **2013**, *250*, 1128−1141.
(51) Allinger, N. L.; Yuh, Y. H.; Lii, J. H. Molecular Mechanics. The MM3 Force Field for Hydrocarbons. 1. *J. Am. Chem. Soc.* **1989**, *111*, 8551−8566.
(52) Lii, J. H.; Allinger, N. L. Molecular Mechanics. The MM3 Force Field for Hydrocarbons. 3. The van der Waals' Potentials and Crystal Data for Aliphatic and Aromatic Hydrocarbons. *J. Am. Chem. Soc.* **1989**, *111*, 8576−8582.
(53) Verstraelen, T.; Vanduyfhuys, L.; Vandenbrande, S.; Rogge, S. M. J. *Yaff, Yet Another Force Field*, http://molmod.ugent.be/software/.
(54) Plimpton, S. Fast Parallel Algorithms for Short-Range Molecular Dynamics. *J. Comput. Phys.* **1995**, *117*, 1−19.
(55) Smith, W.; Forester, T. R. DL_POLY_2.0: A General-Purpose Parallel Molecular Dynamics Simulation Package. *J. Mol. Graphics* **1996**, *14*, 136−141.
(56) Humphrey, W.; Dalke, A.; Schulten, K. VMD: Visual Molecular Dynamics. *J. Mol. Graphics* **1996**, *14*, 33−38.
(57) Kohavi, R. A Study of Cross-Validation and Bootstrap for Accuracy Estimation and Model Selection. *IJCAI'95 Proceedings of the 14th International Joint Conference on Artificial Intelligence*, Volume 2; Morgan Kaufmann: San Francisco, CA, USA, 1995; pp 1137−1143.
(58) Hartigan, J. A. Error Analysis by Replaced Samples. *J. R. Stat. Soc. Series B* **1971**, *33*, 98−110.
(59) Rogge, S. M. J.; Waroquier, M.; Van Speybroeck, V. Reliably Modeling the Mechanical Stability of Rigid and Flexible Metal-Organic Frameworks. *Acc. Chem. Res.* **2018**, *51*, 138−148.

DOI: 10.1021/acs.jctc.7b01134
J. Chem. Theory Comput. XXXX, XXX, XXX−XXX